Rock and Soil Mechanics

Volume 43 | Issue 9 Article 5

11-22-2022

# Influence of particle size distribution and initial dry density on the characteristics of subgrade mud pumping

Yu DING
*School of Civil Engineering, Central South University, Changsha, Hunan 410083, China*

Yu JIA
*School of Civil Engineering, Central South University, Changsha, Hunan 410083, China*

Xuan WANG
*National Engineering Research Centre of High-Speed Railway Construction Technology, Central South University, Changsha, Hunan 410083, China*, dddebug@csu.edu.cn

Jia-sheng ZHANG
*National Engineering Research Centre of High-Speed Railway Construction Technology, Central South University, Changsha, Hunan 410083, China*

*See next page for additional authors*

Follow this and additional works at: https://rocksoilmech.researchcommons.org/journal

 Part of the Geotechnical Engineering Commons

## Custom Citation

DING Yu, JIA Yu, WANG Xuan, ZHANG Jia-sheng, CHEN Xiao-bin, LUO Hao, ZHANG Yu, . Influence of particle size distribution and initial dry density on the characteristics of subgrade mud pumping[J]. Rock and Soil Mechanics, 2022, 43(9): 2539-2549.

This Article is brought to you for free and open access by Rock and Soil Mechanics. It has been accepted for inclusion in Rock and Soil Mechanics by an authorized editor of Rock and Soil Mechanics.

# Influence of particle size distribution and initial dry density on the characteristics of subgrade mud pumping


## Authors

Yu DING, Yu JIA, Xuan WANG, Jia-sheng ZHANG, Xiao-bin CHEN, Hao LUO, and Yu ZHANG



This article is available in Rock and Soil Mechanics: https://rocksoilmech.researchcommons.org/journal/vol43/iss9/5

Rock and Soil Mechanics 2022 43(9): 2539−2549 ISSN 1000−7598
https: //doi.org/10.16285/j.rsm.2021.6971 rocksoilmech.researchcommons.org/journal

# Influence of particle size distribution and initial dry density on the characteristics of subgrade mud pumping

DING Yu[1], JIA Yu[1], WANG Xuan[1, 2], ZHANG Jia-sheng[1, 2], CHEN Xiao-bin[1, 2], LUO Hao[1], ZHANG Yu[1]
1. School of Civil Engineering, Central South University, Changsha, Hunan 410083, China
2. National Engineering Research Centre of High-Speed Railway Construction Technology, Central South University, Changsha, Hunan 410083, China

**Abstract:** The subgrade mud pumping of heavy-haul railway is widespread and harmful, which seriously affects the stability of tracks and the safety of train operation. The properties of railway subgrade soil, such as the particle gradation, the void ratio, have a significant impact on the characteristics of subgrade mud pumping under train load. In this study, a series of remolded samples consisting of silty clay and different content of Kaolin was subjected to mud pumping tests with a self-developed test model. The influence of varying particle gradations (Kaolin content) and initial dry densities (void ratio) on axial strain, excess pore water pressure, and fine particles migration under dynamic load were analyzed. The results show that with the increase in Kaolin content and initial dry density, the axial strain and the excess pore water pressure of the samples, the average migration height of fine particles, and the degree of subgrade mud pumping all decrease. We also find that the excess pore water pressure gradient is the leading factor driving the migration of fine particles in subgrade soil, and the interlayer has a promoting effect on the occurrence of subgrade mud pumping.

**Keywords:** mud pumping; particle size distribution; initial dry density; axial strain; excess pore water pressure; fine particles migration

## 1 Introduction

Economic growth and development requires more and more resources, and railway transportation, especially the heavy-haul railway transportation, has been an important way of achieving this. Compared with ordinary trains, the axle load and traction mass of heavy-haul trains are larger, which aggravates the subgrade diseases, such as mud pumping. The mud pumping of subgrade will not only contaminate the ballast and reduces its drainage performance, but also results in differential settlement of tracks, seriously affecting the track stability and train operation safety[1−2]. The subgrade mud pumping caused by train load is widespread around the world[3−6]. Therefore, it is necessary to study it deeply and systematically.

Mud pumping is widespread, and scholars have conducted a large number of laboratory and field tests on its characteristics, but there are still numerous disputes on its generation and development mechanism. Some scholars believe that the excess pore water pressure (difference) is one of the main causes. Alobaidi et al.[7−10] studied the relationship between the excess pore water pressure between the layers of subgrade structure and the mud pumping under cyclic load. They deemed that the excess pore water pressure between the layers under cyclic load can drive the water to carry fine particles to migrate upward, thus resulting in the mud pumping. Duong et al.[11−12] have concluded by an experimental study that a large excess pore water pressure was generated in the subgrade soil near saturation under cyclic load, and the dissipation of the excess pore water pressure induced the migration of fine particles, thus leading to the mud pumping. However, there was no obvious mud pumping in unsaturated soil. Abeywickrama et al.[13] considered that the excess pore water pressure would be generated and accumulated in undrained railway subgrade under cyclic train load, giving rise to the upward migration of mud and thereby resulting in the mud pumping. Zhang et al.[14−15] carried out the experiment on the hydraulic characteristics of sand-silt mixtures and the migration mechanism of fine particles under the dynamic-static load of trains. By analyzing the deformation and excess pore water pressure of the samples during the test, they stated that the axial pore water pressure gradient inside the samples was the main inducement of migration, flow and accumulation of fine particles. This experiment mainly aimed at the load of high-speed trains, so the stress amplitude of the cyclic load was low, but its frequency was high. Cai et al.[16] conducted an experimental study on the mud pumping mechanism of silty-clay subgrade under traffic load. The results show that the pore water

Received: 24 November 2021 Revised: 6 May 2022
This work was supported by the National Natural Science Foundation of China (51978674).
First author: DING Yu, female, born in 1990, PhD candidate, mainly engaged in the research on the disaster mechanism and prevention of heavy haul railway subgrade diseases. E-mail: ding_yu@csu.edu.cn
Corresponding author: WANG Xuan, male, born in 1977, PhD, Reader, mainly engaged in scientific research and teaching of heavy-haul railway subgrade disease prevention and control. E-mail: dddebug@csu.edu.cn

pressure inside the subgrade accumulates under traffic load; transient liquefaction appears, and mud pumping occurs when the effective stress in the foundation is zero. This experiment was mainly at traffic load, so the stress amplitude of the cyclic load and its frequency were both low. However, Takatoshi[17] believed that the rigidity difference and the incomplete contact between the sleepers and ballast lead to the suction between them when the train is unloaded, and this suction is the main cause of mud pumping. Furthermore, mud pumping has a great relationship with the frost heave of the railway subgrade[18–22] in the seasonal frozen areas in the north and southwest of China.

In this study, according to the stress characteristics of subgrade fills for heavy-haul railways, a mud pumping test model is developed to carry out the research under the load with high cyclic vibration frequency and high stress amplitude. With this model, a series of mud pumping tests was performed on the saturated subgrade soils with different particle gradations and different initial dry densities. The axial strain, the excess pore water pressure and the migration of mud (fine particles) under dynamic load were analyzed to reveal the mud pumping mechanism of saturated subgrade under the train load.

## 2 Test materials and scheme

### 2.1 Test materials

2.1.1 Silty clay

Silty clay was adopted for the tests. Its physical and mechanical parameters were tested according to *Code for soil test of railway engineering* (TB10102—2010)[23], with results shown in Table 1. It can be seen from the table that the silty clay is of low liquid limit. The grading curves of the silty clay are shown in Fig. 1. The figure shows that the content of the silt grains (0.005–0.075 mm[24]) is 58.3% and that of the clay grains (≤0.005 mm[24]) is 29.8%. Figs. 2 and 3 are plotted based on the particle composition and the plasticity index of the studied twenty-four groups of the mud pumping soils[4, 7, 11–12, 16, 20–22, 25–40]. Figures shows that the silty clay used for the tests meets the requirements on the particle composition and the plasticity index of soils prone to mud pumping.

To study the influence of the particle gradation on mud pumping, the commercial Kaolin with particle size of 0.003 4 mm, specific gravity of 2.53, plasticity index of 19.81, maximum dry density of 1.56 g /cm$^3$, and optimum water content of 24.14% was mixed with the original silty clay at a certain percentage to prepare the remolded soils with kaolin contents of 10%, 20% and 30% (Table 1). Commercial kaolin was chosen because this artificial material is easy to be obtained and has stable properties after mixed with other materials[40]. The basic mechanical parameters of the remolded soils are listed in Table 1, and the grading curves are shown in Fig. 1. As shown in the figure, the clay content increases gradually while the silt content decreases gradually with the increase of kaolin content; the plasticity index increases gradually, and the shear strength also increases slightly.

**Table 1 Physical and mechanical parameters of test soils**

| Soil | Particle specific gravity $G_s$ | Liquid Limit $\omega_L$ /% | Plasticity Index $I_P$ | Max. dry density $\rho_{dmax}$ /(g • cm$^{-3}$) | Optimum water content $\omega_{opt}$ /% | Content of silt Grain /% | Content of clay grain /% | Cohesion $c$ /kPa | Internal friction angle $\varphi$/(°) |
|---|---|---|---|---|---|---|---|---|---|
| S | 2.64 | 33.42 | 16.78 | 1.81 | 14.7 | 58.30 | 29.80 | 27.3 | 24.1 |
| 90S10K | 2.62 | 34.33 | 17.02 | 1.76 | 17.4 | 52.47 | 36.82 | 28.3 | 26.6 |
| 80S20K | 2.60 | 36.14 | 17.93 | 1.68 | 20.0 | 46.64 | 43.84 | 30.7 | 25.3 |
| 70S30K | 2.59 | 37.74 | 18.50 | 1.64 | 22.4 | 40.81 | 50.86 | 33.8 | 22.5 |

Note: The cohesion and internal friction angle in the table are obtained through the quick shear test. S represents silty clay, K represents commercial Kaolin. 90S10K, 80S20K, and 70S30K represent the remolded soils with silty clay contents of 90%, 80%, and 70%, and commercial Kaolin contents of 10%, 20%, and 30%, respectively.

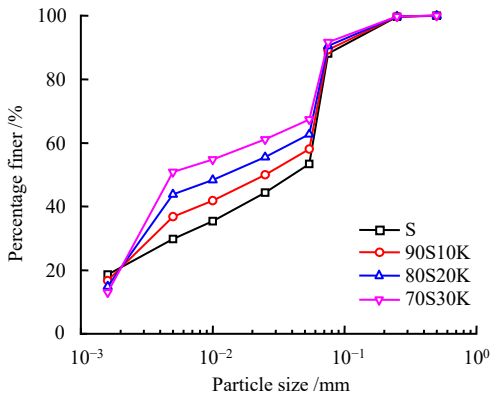


**Fig. 1 Particle grading curves for test soils**

2.1.2 Crushed stone

The crushed stones with particle specific gravity of $G_s$ = 2.69 and the maximum dry density of 2.08 g /cm$^3$ were chosen as ballasts. Due to the limitation of the size of the test instruments, the analogy correction method[41–42]

was used to reduce the scale of the crushed stones. The grading curves of the crushed stones before and after the scale reduction and the upper and lower limits of the ballast grading curve specified in *Railway ballast* (TB/T 2140—2008)[43] are plotted in Fig. 4. The maximum particle size after scale reduction is 30 mm, less than 1/5 of the inner diameter (178 mm) of the sample, and the influence of size effect can be ignored[23−24].

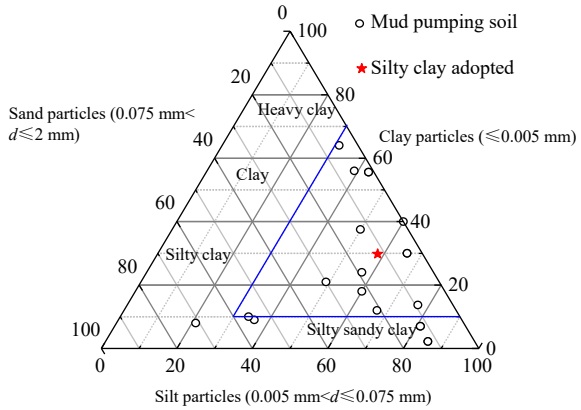


**Fig. 2 Shepard's diagram of particle size distribution for mud pumping soil**

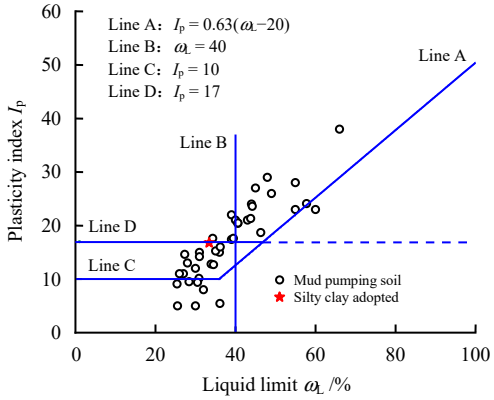


**Fig. 3 Diagram of plasticity index for mud pumping soil**

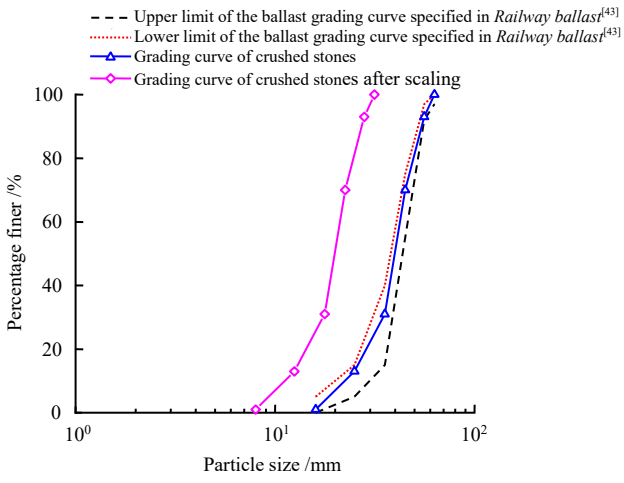


**Fig. 4 Particle grading curves of crushed stones**

## 2.2 Test model and method

### 2.2.1 Test model

The self-developed mud pumping test model consists of four parts: axial loading device (Fig. 5(a)), visual sample cylinder (Fig. 5(b)), sample saturation device (Fig. 5(c)), and data collector (Fig. 5(d)). This model can apply loads with high cyclic vibration frequency and high stress amplitude, observe the mud pumping during the test, collect and record the axial displacement, axial force, pore water pressure, and earth pressure of the sample in real time.

(a) Axial loading device

(b) Visual sample cylinder

(c) Sample saturation device

(d) Data collector

**Fig. 5 Mud pumping test model**

### 2.2.2 Test scheme

The sine wave[44−46] shown in Fig. 6 is used to simulate the train load. Before the dynamic load was applied, an axial static stress of 40 kPa (i.e. $\sigma_p = 40$ kPa) was applied to the sample to simulate the influence of the weight of overlying tracks on ballast[44]. According to the field measured data of Datong–Qinhuangdao railway in literature [46], the dynamic stress on the sleeper of normal section is about 83−113 kPa. The dynamic stress amplitude ($\sigma_d$) selected was 100 kPa. As per the calculation in literature [47], the frequency corresponding to the train speed of 0−100 km /h is 0−14 Hz. Therefore, the loading frequency ($f$) selected was 5 Hz.

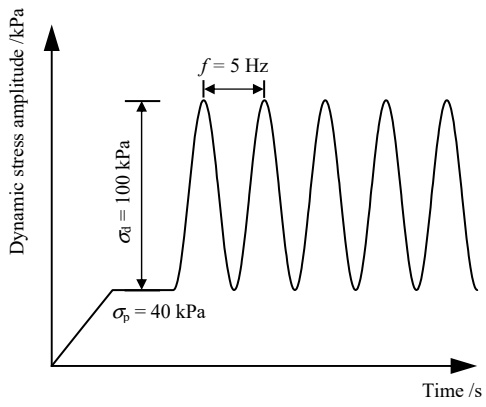


**Fig. 6 Load oscillogram**

The initial dry density of the subgrade soil was controlled as 1.40, 1.50 and 1.59 g /cm$^3$, for the study on its influence on mud pumping. The water content of the subgrade soil was controlled near the optimum water content.

The soil was saturated while the crushed stones were unsaturated during the test. The water in the sample was only allowed to flow along the upper crushed stone layer during loading.

It marks the end of the test when the cyclic loading reaches 50 000 times or the axial strain of the sample reaches 5%.

The testing scheme details are listed in Table 2.

**Table 2 Test scheme**

| No. | Soil type | Initial dry density $\rho_{d0}$ /(g·cm$^{-3}$) | Initial void ratio $e_0$ | Dynamic stress amplitude $\sigma_d$ /kPa | Loading frequency $f$ /Hz |
|---|---|---|---|---|---|
| S-1.40-100-5 | Silty clay | 1.40 | 0.89 | 100 | 5 |
| S-1.50-100-5 | Silty clay | 1.50 | 0.76 | 100 | 5 |
| S-1.59-100-5 | Silty clay | 1.59 | 0.66 | 100 | 5 |
| 90S10K-1.40-100-5 | 90% silty clay + 10% Kaolin | 1.40 | 0.87 | 100 | 5 |
| 90S10K-1.50-100-5 | 90% silty clay + 10% Kaolin | 1.50 | 0.75 | 100 | 5 |
| 90S10K-1.59-100-5 | 90% silty clay + 10% Kaolin | 1.59 | 0.65 | 100 | 5 |
| 80S20K-1.40-100-5 | 80% silty clay + 20% Kaolin | 1.40 | 0.86 | 100 | 5 |
| 80S20K-1.50-100-5 | 80% silty clay + 20% Kaolin | 1.50 | 0.73 | 100 | 5 |
| 80S20K-1.59-100-5 | 80% silty clay + 20% Kaolin | 1.59 | 0.64 | 100 | 5 |
| 70S30K-1.40-100-5 | 70% silty clay + 30% Kaolin | 1.40 | 0.85 | 100 | 5 |
| 70S30K-1.50-100-5 | 70% silty clay + 30% Kaolin | 1.50 | 0.73 | 100 | 5 |
| 70S30K-1.59-100-5 | 70% silty clay + 30% Kaolin | 1.59 | 0.63 | 100 | 5 |

Note: No. S-1.40-100-5 means that the initial dry density of silty clay is 1.40 g /cm$^3$, the dynamic stress amplitude is 100 kPa, the loading frequency is 5 Hz, and so on.

2.2.3 Sample preparation

The sample was 178 mm (diameter) × 380 mm (height). The lower part of the sample was filled with silty clay (subgrade soil), with a height of 250 mm; the upper part was filled with crushed stones (ballast), with a height of 130 mm. Two pieces of filter paper were laid on the cylinder bottom and vaseline was evenly spread on the cylinder side wall before the sample preparation. Vaseline can reduce the friction between the soil and the side wall, and can also prevent, to a certain extent, the concentrated seepage of water along the side wall in the process of soil saturation, which affects the saturation effect. The silty clay was filled by the layered compaction method and divided into 5 layers, each with a thickness of 50 mm. Before the next layer was filled, roughen the surface of the compacted previous layer to ensure good contact between the layers. During sample preparation, three pore water pressure sensors (Type BWMK) and three earth pressure sensors (BW earth pressure box) were embedded in the soil. The sensors were 240, 160, and 80 mm away from the sample bottom, represented by Point *A* (240 mm), Point *B* (160 mm), and Point *C* (80 mm). The upper crushed stones were filled in three layers, each with a thickness of 50, 50 and 30 mm.

The sample was saturated after preparation. It was evacuated by a vacuum pump. Then the water inlet valve at the bottom of the cylinder was opened to make the water flow into the soil slowly and then was closed when the water surface inside is 10 mm higher than the soil surface. Loading started after the sample stood for 24 hours. It was learnt from the previous test that the saturation of subgrade soil could reach about 85% by using this method, and its height would not change a lot before and after saturation.

## 3 Analysis and discussion

### 3.1 Typical curves

Figure 7 shows the curves of the axial strain (ratio of axial deformation to initial height), the excess pore water pressure, and the soil dynamic stress with cyclic number of sample S-1.40-100-5. And Fig. 8 shows changes

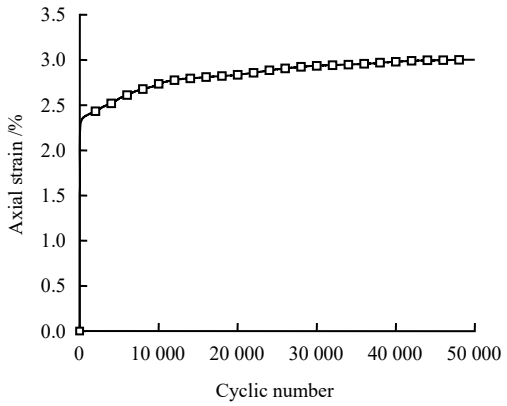


(a) Axial strain–vibration curve

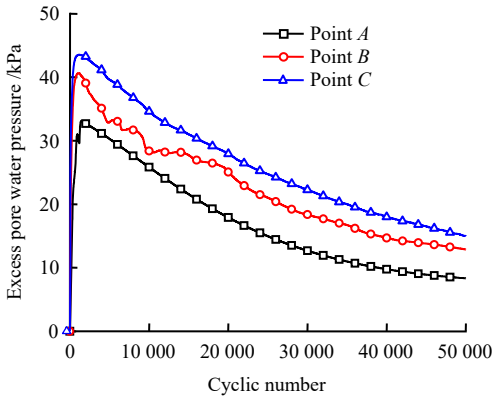


(b) Excess pore water pressure–vibration curve

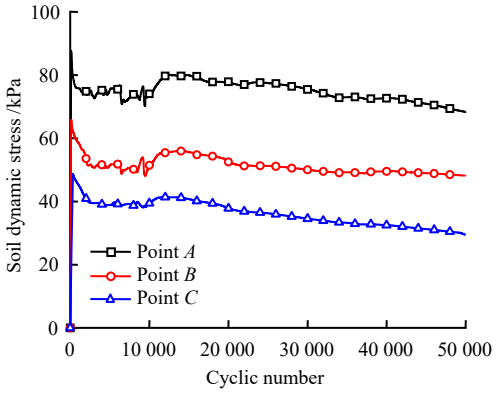


(c) Soil dynamic stress–vibration curve

**Fig. 7 Typical curves for sample S-1.40-100-5**

of the interface between the soil and the crushed stones during the test. Fig. 7(a) shows that the axial strain increases nonlinearly with increasing the cyclic number, and the increase rate gradually decreases. According to the interface changes shown in Fig. 8, the axial deformation of the sample mainly originates from two aspects: (1) The crushed stone layer sank into the silty clay layer under dynamic load and formed an interlayer with a certain thickness. The interlayer mainly occurs at the initial stage of dynamic loading. Therefore, when the cyclic number is less than 1 000, the axial strain increases almost linearly and rapidly. (2) The axial deformation increases gradually with the dissipation of the excess pore water pressure (Fig. 7(b)) and the upward migration of fine particles (mud).

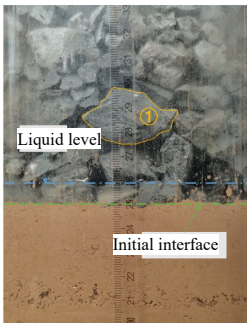


(a) when the sample is saturated

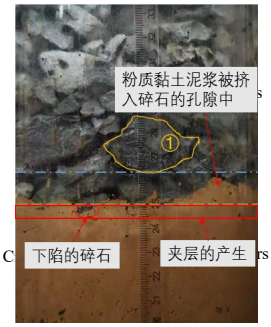


(b) when the dynamic load is applied

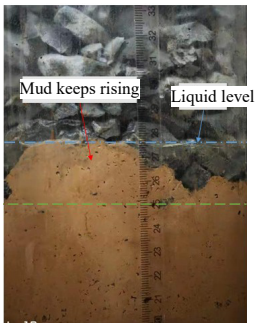


(c) when the test is ended

**Fig. 8 Changes of interface of subgrade soil and crushed stones for sample S-1.40-100-5**

Figure 7(b) shows that the excess pore water pressure increases rapidly and then decreases slowly with increasing the cyclic number. Under the external force, a large axial strain is generated, and the soil is squeezed, resulting in a large excess pore water pressure. Water was allowed to flow along the pores of the upper crushed stones during the test. Therefore, the excess pore water pressure dissipated slowly, the free liquid level rose gradually, and the mud also migrated upward.

It can be seen from Fig. 7(c) that the soil dynamic stress tends to decrease gradually in general with increasing the cyclic number. The soil dynamic stress corresponding to the same cyclic number decreases gradually with increasing the soil depth, indicating that the influence of external forces on the soil decreases gradually with the depth.

The evolution of the excess pore water pressure under cyclic load has an important influence on the subgrade mud pumping. Fig. 9 shows the time history curve of the excess pore water pressure at point *B* of sample S-1.40-100-5. Due to the large amount of data, the figure only

shows the excess pore water pressure within 0−1 000 s. Learnt from Fig. 9, the excess pore water pressure accumulates and increases rapidly when the cyclic load is applied. The excess pore water pressure increases approximately linearly in the first 10 s. The growth rate decreases gradually within 10−20 s. The excess pore water pressure reaches the peak with loading for about 170 s. The dissipation of the excess pore water pressure starts to play a main role, and it decreases little by little, when loading is for more than 170 s. The figure also shows that the excess pore water pressure changes in the form of sine wave with the application of the external load, but the amplitude is very small.

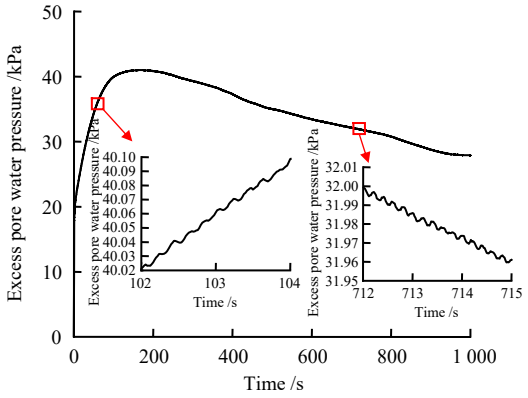


**Fig. 9 Time history curve of excess pore water pressure at point *B* for sample S-1.40-100-5**

## 3.2 Influence of particle gradation on mud pumping

In this section, the influence of particle gradation of subgrade soil on mud pumping is analyzed from four aspects, i.e., the axial strain, the excess pore water pressure, the average height of fine particles (mud) migration during the test, and the change of particle grading curves of crushed stones after the test.

### 3.2.1 Axial strain

Figure 10 shows the axial strain–cyclic number curves of the samples with different gradations. In the tests of sample S, 90S10K and 80S20K, the axial strain increases rapidly at first and then slowly with increasing the cyclic number. Until the end of the test, the axial deformation is still not stable. However, the axial strain of sample 70S30K shows different trends, that is, the axial strain increases rapidly at first and then remains stable with increasing the cyclic number. The axial strain corresponding to the same cyclic number also decreases gradually with the increase of kaolin (clay) content. This finding differs from that in reference [16]. The reason may be explained as follows. (1) The soil used in reference [16] (silty clay composed of silt and kaolin) is different from that in this study. (2) The kaolin content used to analyze its influence on the sample deformation in reference [16] is different from that in this study: high kaolin content (>60%) in reference [16] while low kaolin content (⩽30%) in this study. Indraratna et al.[40] studied the deformation of the mixtures of kaolin (10% and 30%) and sandy clay under the cyclic load, and get the conclusions similar to those in this study. In addition, learnt from Table 2, the increase of kaolin content reduces the initial void ratio gradually, which makes the sample more compact inside. Therefore, the deformation induced by the external load also reduces gradually.

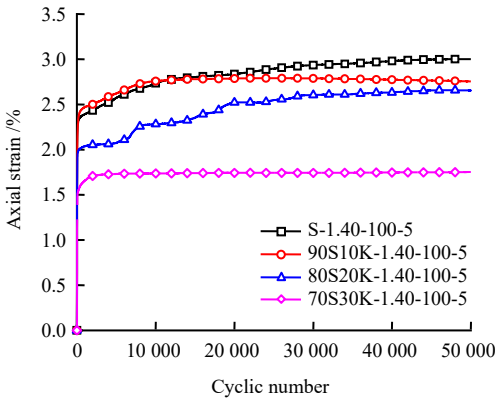


**Fig. 10 Influence of particle gradation on axial strain**

### 3.2.2 Excess pore water pressure

Figure 11 shows the influence of particle gradation on the excess pore water pressure. Due to the space limitation, only the curve of the excess pore water pressure at Point *B* is plotted here. It can be observed from the figure that the excess pore water pressure curves of the soils with four different particle gradations all change consistently,

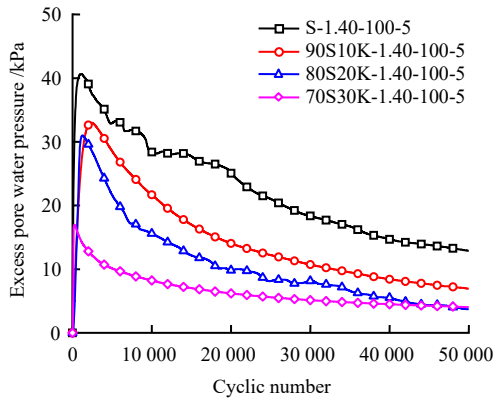


**Fig. 11 Influence of particle gradation on excess pore water pressure at point *B***

that is, with increasing the cyclic number, they first increase rapidly and then decrease gradually. The increase of kaolin content can lead to the gradual decrease of the excess pore water pressure and its peak value under dynamic load. For instance, when the kaolin content increased from 0 to 10%, 20% and 30%, the peak excess pore water pressure of the sample with an initial dry density of 1.40 g /cm$^3$ at point *B* decreased from 40.6 kPa to 32.9, 30.9, and 16.9 kPa. With the increase of kaolin content, the initial dry density decreases, and the sample becomes more compact. The accumulated excess pore water pressure inside also becomes smaller under the same cyclic number.

3.2.3 Average migration height of fine particles (mud)

Four reference points were selected and the heights of fine particles (mud) corresponding to different loading times were recorded during test, and the averages of the mud heights at the four reference points were used for analysis. Table 3 gives the average mud height of soils with different particle gradations under different cyclic numbers, where *N* refers to the cyclic vibration number. Learnt from Table 3, the average mud height increases gradually with increasing the cyclic number, but the increase rate of the average height decreases gradually. Mud migration under cyclic load mainly occurs at the early stage, i.e. when the cyclic number is less than 15 000. According to the test results, it is found that on the one hand the mud migration is caused by the subsidence of the crushed stone layer, which pushes the soil into the upper crushed stone layer; on one hand, by driving effect of the excess pore water pressure[12]. Table 3 also displays that the addition of kaolin significantly reduces the average mud height and restrains the subgrade mud pumping.

**Table 3 Average mud height and mud mass**

| No. | Average height /mm | | | | Mass /g |
|---|---|---|---|---|---|
| | $N$ = 1 000 | $N$ = 15 000 | $N$ = 30 000 | $N$ = 50 000 | |
| S-1.40-100-5 | 14.75 | 21.00 | 23.00 | 24.75 | 422.8 |
| S-1.50-100-5 | 14.50 | 15.75 | 16.25 | 17.00 | 166.2 |
| S-1.59-100-5 | 3.75 | 6.25 | 7.75 | 7.75 | 115.1 |
| 90S10K-1.40-100-5 | 9.50 | 13.75 | 14.50 | 15.00 | 300.1 |
| 90S10K-1.50-100-5 | 10.00 | 11.75 | 12.75 | 13.50 | 145.8 |
| 90S10K-1.59-100-5 | 2.75 | 3.50 | 4.00 | 4.25 | 85.7 |
| 80S20K-1.40-100-5 | 9.00 | 11.50 | 12.00 | 12.25 | 214.2 |
| 80S20K-1.50-100-5 | 8.25 | 8.75 | 9.25 | 10.00 | 100.7 |
| 80S20K-1.59-100-5 | 2.00 | 2.00 | 2.50 | 2.50 | 44.8 |
| 70S30K-1.40-100-5 | 9.50 | 10.00 | 10.50 | 11.00 | 158.9 |
| 70S30K-1.50-100-5 | 5.50 | 6.25 | 6.75 | 7.00 | 101.1 |
| 70S30K-1.59-100-5 | 1.00 | 1.00 | 1.00 | 1.00 | 26.7 |

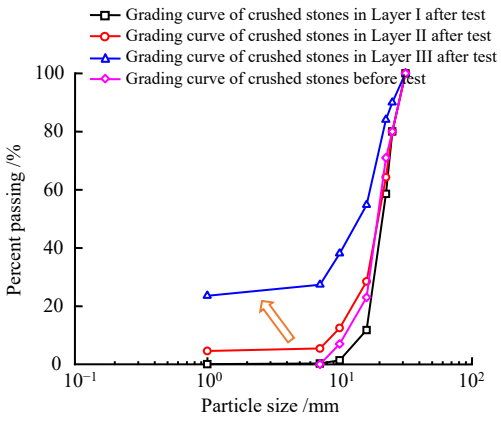


(a) S-1.40-100-5

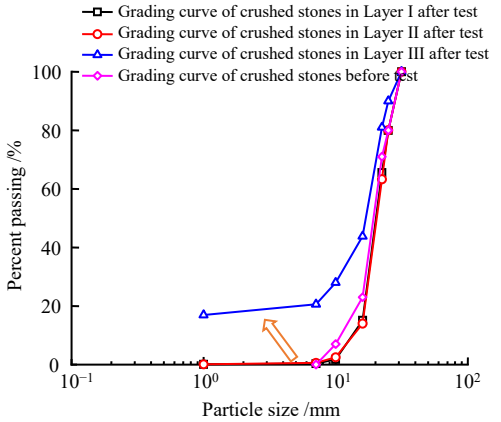


(b) 90S10K-1.40-100-5

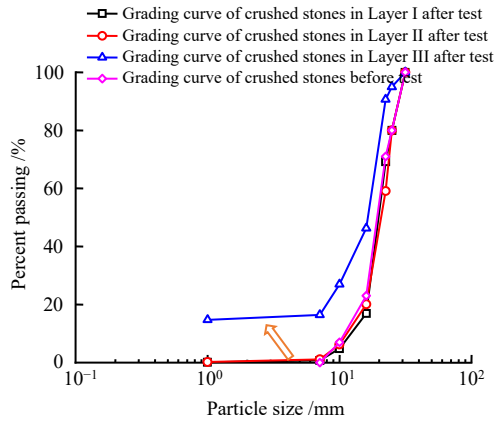


(c) 80S20K-1.40-100-5

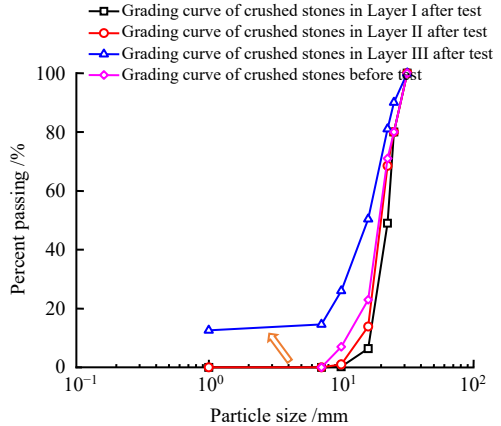


(d) 70S30K-1.40-100-5

**Fig. 12 Grading curves of crushed stones after test**

3.2.4 Grading curve of crushed stones

After the test, the upper crushed stones were taken out in three layers, 50 mm thick for the upper two layers (Layer I and Layer II) and 30 mm thick for the bottom layer (Layer III). The washing method was adopted to obtain the mud mass in the upper crushed stone layers. Firstly, the crushed stones with mud were dried and weighed. Then they were washed on a sieve with an aperture size of 1 mm to remove the fine particles less than 1 mm (mainly the subgrade fine particles adhering to the crushed stones; secondly, a small number of fine particles are produced by the ballast wear during loading, which is not distinguished because of the small quantity.) The particles left on the sieve were dried and weighed again. The mass difference is the mass of the mud adhering to the crushed stones each layer (as shown in Table 3). Finally, the particle analysis tests were carried out on the fried clean crushed stones. Fig. 12 shows the particle grading curves of the crushed stones each layer after the test. According to Fig. 12, the grading curves of the crushed stones in Layer I and Layer II basically don't change after the test, compared with the grading curve before the test, which indicates that there was basically no or only a small amount of mud accumulated in Layer I and Layer II after the test. However, the particle grading curve of the crushed stones in Layer III obviously deviates to the upper left, and the content of particles with size less than 1 mm increases significantly, indicating that a large amount of mud from the subgrade is accumulated in Layer III. With the comparison of the grading curves of the crushed stones in Layer III in different kaolin content tests, it is found that the deviation of the particle grading curve of Layer III crushed stones decreases with the increase of kaolin content, and the mass of the mud in the crushed stones also decreases, indicating that the mud pumping is restrained gradually.

### 3.3 Influence of initial dry density on mud pumping

3.3.1 Axial strain

Figure 13 shows the influence of the initial dry density on the axial strain. It can be seen from the figure that the axial strain decreases with the increase of the initial dry density of the soil. As shown in Table 2, the initial dry density of the silty clay increases from 1.40 g /cm$^3$ to 1.50 and 1.59 g /cm$^3$ while the corresponding initial void ratio decreases from 0.89 to 0.76 and 0.66. Void ratio decreasing means that soil becomes more compact and stronger. As a result, the subsidence depth of the upper crushed stones into the subgrade soil (i.e. the interlayer thickness) decreases, as well as the sample axial deformation, under external load.

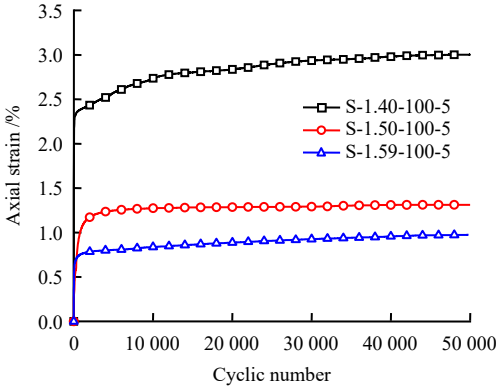


**Fig. 13 Influence of initial dry density on curves of axial strain and cyclic number**

3.3.2 Excess pore water pressure

The influence of the initial dry density of subgrade soil on the excess pore water pressure at Point *B* is shown in Fig. 14. It can be seen that the excess pore water pressure decreases with increasing of the initial dry density. Increasing of the initial dry density reduces the void ratio of subgrade soil and the compressive deformation under external load, as well as the excess pore water pressure generated inside the sample correspondently.

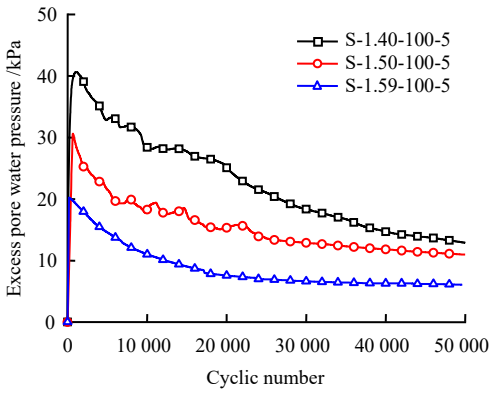


**Fig. 14 Influence of initial dry density on curves of excess pore water pressure and cyclic number at point *B***

3.3.3 Average migration height and mass of fine particles (mud)

The influence of the initial dry density on the average height and mass of the migrated mud is shown in Table 3. As shown in Table 3, the increase in the dry density of subgrade soil significantly reduces the average height and mass of the migrated mud and restrains mud pumping. Increasing of the initial dry density of subgrade soil makes the internal structure of the soil more compact. Under external load, the subgrade soils, especially those in contact with the crushed stones, are difficult to be soften to mud.

Therefore, the average height and migration mass of the mud are also significantly reduced.

## 4 Mud pumping mechanism

Mud pumping of the saturated subgrade under dynamic load is caused by the drive of excess pore water pressure. Here, the concept of excess pore water pressure gradient is introduced[48], which can be calculated as below:

$$i_{\mathrm{d}}=\frac{H_{\mathrm{d}i}-H_{\mathrm{d}j}}{L_{ij}} \tag{1}$$

where $i_{\mathrm{d}}$ is the excess pore water pressure gradient; $H_{\mathrm{d}i}$ and $H_{\mathrm{d}j}$ is the water head corresponding to the excess pore water pressure at Point *i* and Point *j*, respectively; $L_{ij}$ is the distance between Point *i* and Point *j*. The excess pore water pressure gradient at Point *B* and Point *A* (*B*−*A*) and the excess pore water pressure gradient at Point *C* and Point *B* (*C*−*B*) of Sample S-1.40-100-5 are calculated according to Eq. 1 and plotted in Fig. 15. As can be seen from Fig. 15, the excess pore water pressure gradient trends to decrease with the increase of cyclic vibration frequency. The excess pore water pressure gradient at *B*−*A* is still greater than 6.0 at the end of loading, which is sufficient to drive the migration of fine particles[49−51].

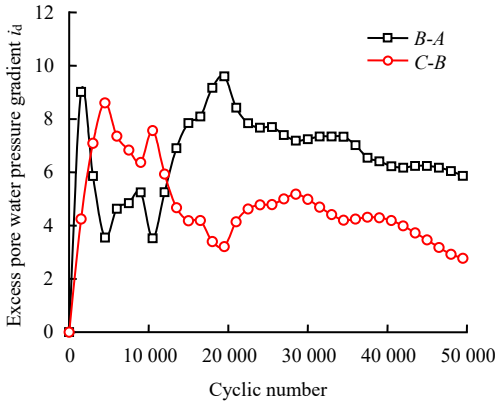


**Fig. 15 Curves of excess pore water pressure gradient and cyclic number**

Figure 15 also shows that the excess pore water pressure at *B*−*A* is generally larger than the one at *C*−*B*, indicating that the migration of fine particles mainly occurs in the middle and upper part of subgrade soil.

Furthermore, the subgrade mud pumping is often accompanied by the generation of the interlayer, and the larger the thickness of the interlayer, the larger the axial deformation, the excess pore water pressure, and the mud average height of the sample also increase accordingly. In other words, the generation of interlayer can boost the evolution of subgrade mud pumping[14].

## 5 Conclusion

In this study, the mud pumping test was conducted on saturated soils with different particle gradations and initial dry densities, and the axial strain, excess pore water pressure, and fine particle (mud) migration under dynamic load were analyzed. The following conclusions were drawn:

(1) The axial strain increases nonlinearly with increasing of the cyclic number, and the increase rate decreases gradually. The axial deformation comes from two aspects: (i) formation of the interlayer; (ii) dissipation of the excess pore water pressure and the compression deformation caused by the fine particle (mud) migration. The excess pore water pressure has a trend of rapid increase firstly and gradual decrease then with increasing the cyclic number while the soil dynamic stress decreases gradually.

(2) The increase of kaolin content reduces the axial strain and the excess pore water pressure, and the average height of the mud. This finding indicates that appropriate changes in the particle gradation of the soil can alleviate the severity of subgrade mud pumping.

(3) The void ratio of the subgrade soil gradually decreases, and the internal structure of the sample becomes more compact with the increase of the initial dry density. Therefore, the axial strain and the excess pore water pressure decrease under dynamic load. The increase of the initial dry density of subgrade soil can restrain the occurrence of subgrade mud pumping to a certain extent.

(4) The excess pore water pressure gradient inside the sample under dynamic load is the dominant factor in the migration of fine particles of subgrade soil, and the interlayer formed during the test can boost the evolution of subgrade mud pumping.

## References

[1] SELIG E T, WATERS J M. Track geotechnology and substructure management[M]. London: Thomas Telford, 1994.

[2] INDRARATNA B, FERREIRA F B, QI Y, et al. Application of geoinclusions for sustainable rail infrastructure under increased axle loads and higher speeds[J]. Innovative Infrastructure Solutions, 2018, 3(1): 1−21.

[3] LIU S S, HUANG H, QIU T, et al. Characterization of ballast particle movement at mud spot[J]. Journal of Materials in Civil Engineering, 2019, 31(1): 04018339.

[4] INDRARATNA B, RUJIKIATKAMJORN C, EWERS B,

et al. Class A prediction of the behavior of soft estuarine soil foundation stabilized by short vertical drains beneath a rail track[J]. Journal of Geotechnical and Geoenvironmental Engineering, 2010, 136(5): 686−696.

[5] HAYASHI S, SHAHU J T. Mud pumping problem in tunnels on erosive soil deposits[J]. Geotechnique, 2000, 50(4): 393−408.

[6] FU H L, LI K, HE Y W, et al. The field study of the remediation of mud-pumping[J]. Advanced Materials Research, 2012, 430−432(3): 2079−2082.

[7] ALOBAIDI I, HOARE D J. Mechanisms of pumping at the subgrade-subbase interface of highway pavements[J]. Geosynthetics International, 1999, 6(4): 241−259.

[8] ALOBAIDI I, HOARE D J. The role of geotextile reinforcement in the control of pumping at the subgrade-subbase interface of highway pavements[J]. Geosynthetics International, 1998, 5(6): 619−636.

[9] ALOBAIDI I, HOARE D J. Qualitative criteria for anti-pumping geocomposites[J]. Geotextiles and Geomembranes, 1998, 16(4): 221−245.

[10] ALOBAIDI I, HOARE D J. Factors affecting the pumping of fines at the subgrade subbase interface of highway pavements: a laboratory study[J]. Geosynthetics International, 1994, 1(2): 221−259.

[11] DUONG T V, CUI Y J, TANG A M, et al. Physical model for studying the migration of fine particles in the railway substructure[J]. Geotechnical Testing Journal, 2014, 37(5): 895−906.

[12] DUONG T V, CUI Y J, TANG A M, et al. Investigating the mud pumping and interlayer creation phenomena in railway sub-structure[J]. Engineering Geology, 2014, 171: 45−58.

[13] ABEYWICKRAMA A, INDRARATNA B, RUJIKIATKAMJORN C. Excess pore-water pressure generation and mud pumping in railways under cyclic loading[J]. Lecture Notes in Civil Engineering, 2019, 28: 371−383.

[14] ZHANG Sheng, GAO Feng, CHEN Qi-lei, et al. Experimental study of fine particles migration mechanism of sand-silt mixtures under train load[J]. Rock and Soil Mechanics, 2020, 41(5): 1591−1598.

[15] ZHANG S, GAO F, HE X Z, et al. Experimental study of particle migration under cyclic loading: effects of load frequency and load magnitude[J]. Acta Geotechnica, 2021, 16(2): 367−380.

[16] CAI Yuan-qiang, YAN Shu-hao, CAO Zhi-gang, et al. Experiments to investigate mechanism of mud pumping of road base on silty clay soil under cyclic loading[J]. Journal of Jilin University (Engineering and Technology Edition), 2021, 51(5): 1742−1748.

[17] TAKATOSHI I. Measures for stabilization of railway earth structures[R]. Tokyo: Japan Railway Technical Service, 1997.

[18] ZHANG S, SHENG D C, ZHAO G T, et al. Analysis of frost heave mechanisms in a high-speed railway embankment[J]. Canadian Geotechnical Journal, 2016, 53(3): 520−529.

[19] SHENG D C, ZHANG S, NIU F, et al. A potential new frost heave mechanism in high-speed railway embankments[J]. Geotechnique, 2014, 64(2): 144−154.

[20] LIU Jun-sheng. Research on the remediation of seasonal foundation bed with mud pumping[J]. Subgrade Engineering, 2005(4): 102−104.

[21] GU Xian-ming. Study on mechanism and prevention of frost heaving and frost boiling in seasonally frozen road[D]. Changchun: Jilin University, 2007.

[22] GUO Sheng. Treatment of frost-heaving and mud pumping caused by spring thaw for Beijing-Tongliao railway subgrade[J]. Railway Engineering, 2016(11): 101−103.

[23] China Railway First Survey and Design Institute Group Co. Ltd. TB10102−2010 Code for soil test of railway engineering[S]. Beijing: China Railway Publishing House Co., Ltd., 2010.

[24] Nanjing Hydraulic Research Institute. SL237 − 1999 Specification of soil test[S]. Beijing: China Water and Power Press, 1999.

[25] CHAWLA S, SHAHU J T. Reinforcement and mud-pumping benefits of geosynthetics in railway tracks: model tests[J]. Geotextiles and Geomembranes, 2016, 44(3): 366−380.

[26] TRINH V N, MINHTANG A, CUI Y, et al. Mechanical characterization of the fouled ballast in ancient railway track substructure by large-scale triaxial tests[J]. Soils and Foundations, 2012, 52(3): 511−523.

[27] VOOTTIPRUEX P, ROONGTHANEE J. Prevention of mud pumping in railway embankment: a case study from Baeng Pra-Pitsanuloke, Thailand[J]. International Journal of Applied Science and Technology, 2003, 13(1): 20−25.

[28] KAMRUZZAMAN A H M, HAQUE A, BOUAZZA A. Filtration behaviour of granular soils under cyclic load[J]. Geotechnique, 2008, 58(6): 517−522.

[29] TRANI L D O, INDRARATNA B. Assessment of subballast filtration under cyclic loading[J]. Journal of Geotechnical and Geoenvironmental Engineering, 2010, 136(11): 1519−1528.

[30] TRANIO L D O, INDRARATNA B. Experimental investigations into subballast filtrations behaviour under cyclic conditions[J]. Australian Geomechanics, 2010, 45(3): 123−133.

[31] KOOHMISHI M, AZARHOOSH A. Assessment of drainage

and filtration of sub-ballast course considering effect of aggregate gradation and subgrade condition[J]. Transportation Geotechnics, 2020, 24: 100378.

[32] ESMAEILI M, SALAJEGHEH M, FAMENIN S J. Experimental assessment of geotextile serviceability lifetime as ballasted railway filter focusing on clogging phenomenon[J]. Construction and Building Materials, 2019, 211: 675−687.

[33] HASNAYN M M, MCCARTER W J, WOODWARD P K, et al. Railway subgrade performance after repeated flooding-large-scale laboratory testing[J]. Transportation Geotechnics, 2020, 23: 100329.

[34] HASNAYN M M, MCCARTER W J, WOODWARD P K, et al. Railway subgrade performance during flooding and the post-flooding (recovery) period[J]. Transportation Geotechnics, 2017, 11: 57−68.

[35] INDRARATNA B, ATTYA A, RUJIKIATKAMJORN C. Experimental investigation on effectiveness of a vertical drain under cyclic loads[J]. Journal of Geotechnical and Geoenvironmental Engineering, 2009, 135: 835−839.

[36] MIAO Xiao-qi. Analysis on reason of defects in Jiuyanshan tunnel and suggestion of measures for their regulation[J]. Journal of Railway Engineering Society, 2003(2): 70−72.

[37] ZHAO Man-qing. Study on disease control of fissured soil foundation bed[D]. Chengdu: Southwest Jiaotong University, 2002.

[38] WU Xin-ming. Analysis on shoulder of road pushing of Nankun railway and lab. research of improved soil[D]. Chengdu: Southwest Jiaotong University, 2007.

[39] YANG Xin-an. Railroad substructure and problem of Yuntaishan tunnel inspection using GPR[J]. Bulletin of Geological Science and Technology, 2002(4): 86−88.

[40] INDRARATNA B, KORKITSUNTORNSAN W, NGUYEN T T. Influence of Kaolin content on the cyclic loading response of railway subgrade[J]. Transportation Geotechnics, 2020, 22: 100319.

[41] INDRARATNA B, WIJEWARDENA L S S, BALASUBRAMANIAM A S. Large-scale triaxial testing of greywacke rockfill[J]. Géotechnique, 1993, 43(1): 37−51.

[42] WANG Han-lin. Mechanical characterization and moisture migration of the high-speed railway track-bed[D]. Hangzhou: Zhejiang University, 2017.

[43] China Academy of Railway Sciences. TB/T 2140−2008 Railway ballast[S]. Beijing: China Railway Publishing House Co., Ltd., 2008.

[44] BIAN X C, JIANG J Q, JIN W F, et al. Cyclic and polycyclic triaxial testing of ballast and subballast[J]. Journal of Materials in Civil Engineering, 2016, 28(7): 4016032.

[45] DING Y, ZHANG J S, CHEN X B, et al. Experimental investigation on static and dynamic characteristics of granulated rubber-sand mixtures as a new railway subgrade filler[J]. Construction and Building Materials, 2021, 273: 121955.

[46] YANG Zhi-hao. Research on the mechanism of mud pumping of heavy haul-railways[D]. Shijiazhuang: Shijiazhuang Tiedao University, 2015.

[47] SUN Q D, INDRARATNA B, NIMBALKAR S. Deformation and degradation mechanisms of railway ballast under high frequency cyclic loading[J]. Journal of Geotechnical and Geoenvironmental Engineering, 2016, 142(1): 4015056.

[48] ARIVALAGAN J, RUJIKIATKAMJORN C, INDRARATNA B, et al. The role of geosynthetics in reducing the fluidization potential of soft subgrade under cyclic loading[J]. Geotextiles and Geomembranes, 2021, 49(5): 1324−1338.

[49] INDRARATNA B, ISRAR J, RUJIKIATKAMJORN C. Geometrical method for evaluating the internal instability of granular filters based on constriction size distribution[J]. Journal of Geotechnical and Geoenvironmental Engineering, 2015: 10.1061/(ASCE)GT.1943-5606.0001343.

[50] ISRAR J, INDRARATNA B. Study of critical hydraulic gradients for seepage-induced failures in granular soils[J]. Journal of Geotechnical and Geoenvironmental Engineering, 2019, 145(7): 04019025.

[51] STERPI D. Effects of the erosion and transport of fine particles due to seepage flow[J]. International Journal of Geomechanics, 2003, 3(1): 111−122.